PLEASE CITE THIS ARTICLE AS DOI: 10.1063/5.0044702

AP Publishing

Compositional and Phase Dependence of Elastic Modulus of Crystalline and Amorphous $Hf_{1-x}Zr_xO_2$ Thin Films Shelby S. Fields. David H. Olson, Samantha T. Jaszewski, Chris M. Fancher,

Shelby S. Fields, ¹ David H. Olson, ² Samantha T. Jaszewski, ¹ Chris M. Fancher, ³ Sean W. Smith, ^{4,*} Diane A. Dickie, ^{1,5} Giovanni Esteves, ⁴ M. David Henry, ⁴ Paul S. Davids, ⁴ Patrick E. Hopkins, ^{1, 2, 6} and Jon F. Ihlefeld^{1, 7, †}

The elastic moduli of amorphous and crystalline atomic layer-deposited $Hf_{1-x}Zr_xO_2$ (HZO, x=0, 0.31, 0.46, 0.79, 1) films prepared with TaN electrodes on silicon substrates were investigated using picosecond acoustic measurements. The moduli of the amorphous films were observed to increase between 211 \pm 6 GPa for pure HfO_2 and 302 ± 9 GPa for pure ZrO_2 . In the crystalline films it was found that the moduli increased with increasing zirconium composition from 248 \pm 6 GPa for monoclinic HfO_2 , to 267 \pm 9 GPa for tetragonal ZrO_2 . Positive deviations from this increase were observed for the $Hf_{0.69}Zr_{0.31}O_2$ and $Hf_{0.54}Zr_{0.46}O_2$ compositions, which were measured to have moduli of 264 ± 8 GPa and 274 ± 8 GPa, respectively. These two compositions contained the largest fractions of the ferroelectric orthorhombic phase, as assessed from polarization and diffraction data. The biaxial stress states of the crystalline films were characterized through $\sin^2(\psi)$ X-ray diffraction analysis. The in-plane stresses were all found to be tensile and observed to increase with increasing zirconium composition, between 2.54 \pm 0.6 GPa

¹Department of Materials Science and Engineering, University of Virginia, Charlottesville, Virginia, USA 22904

²Department of Mechanical and Aerospace Engineering, University of Virginia, Charlottesville, Virginia, USA 22904

³Materials Science and Technology Division, Oak Ridge National Laboratory, Oak Ridge, Tennessee, USA 37831

⁴Sandia National Laboratories, Albuquerque, New Mexico, USA 87185

⁵Department of Chemistry, University of Virginia, Charlottesville, Virginia, USA 22904

⁶Department of Physics, University of Virginia, Charlottesville, Virginia, USA 22904

⁷Charles L. Brown Department of Electrical and Computer Engineering, University of Virginia, Charlottesville, Virginia, USA 22904

^{*} Current address: Radiant Technologies

[†] jihlefeld@virginia.edu

ACCEPTED MANUSCRIPT

Applied Physics Letters



This is the author's peer reviewed, accepted manuscript. However, the online version of record will be different from this version once it has been copyedited and typeset.

PLEASE CITE THIS ARTICLE AS DOI: 10.1063/5.0044702

for pure HfO_2 and 5.22 ± 0.5 GPa for pure ZrO_2 . The stresses are consistent with large thermal expansion mismatches between the HZO films and silicon substrates. These results demonstrate a device-scale means to quantify biaxial stress for investigations on its effect on the ferroelectric properties of hafnia-based materials.

PLEASE CITE THIS ARTICLE AS DOI: 10.1063/5.0044702

Since the first reporting of ferroelectric responses nearly a decade ago, HfO₂-based thin films have witnessed research and development for applications including ferroelectric random access memory,²⁻⁵ energy harvesting,^{6,7} and negative differential capacitance field effect transistors.^{8,9} The ferroelectric response has been attributed to a non-centrosymmetric orthorhombic phase (space group Pca21), which is energetically metastable between the roomtemperature, linear dielectric monoclinic $(P2_1/c)$ and high-temperature field-induced-ferroelectric tetragonal (P42nmc) phases. 10,11 The stability of this orthorhombic phase has been attributed to small crystallite sizes, ¹² inclusion of specific dopants, ^{13,14} and the presence of biaxial stress, ^{15,16} among others. HfO₂-based ferroelectrics are typically grown to thicknesses of 5 – 20 nm, which limits the grain size via thickness truncation, and doped to enhance orthorhombic phase stability. ZrO2 alloying has been observed to stabilize the orthorhombic phase through a broad composition window ($x \approx 0.1 - 0.8$)^{17,18} and result in a reduced thermal budget compared to many other ferroelectric HfO₂ compositions. 19,20 In spite of the many mechanisms to increase orthorhombic phase stability, Hf_{1-x}Zr_xO₂ (HZO) thin films often exhibit mixtures of the orthorhombic, tetragonal, and monoclinic phases, with Hf-rich and Zr-rich compositions resulting in monoclinic-rich and tetragonal-rich phase constitutions, respectively. 17,18,21,22

Biaxial stress impacts both the phase stability and the domain structure. Computational works have suggested that compressive biaxial stresses facilitate stabilization of the orthorhombic phase compared to the equilibrium monoclinic.¹¹ Experimental studies, alternatively, have observed enhanced polarization responses under conditions that yield biaxial tensile stress, ^{16,23} or favorable texture, ²⁴ both of which alter the domain structure to maximize the degree to which the short polar axis is oriented normal to the film surface. Such experimental works examining stress effects in HfO₂-based ferroelectrics rely on combinations of experimental and computationally predicted bulk elastic constants for the monoclinic, tetragonal, and orthorhombic phases for analysis. Measurement of these values in planar, mixed phase thin films is important because utilization of bulk, phase-pure elastic constants may discount effects of microstructural features such as the high density of grain boundaries and presence of interface segregated phases, ^{18,25} both of which may affect the elastic properties. Thus, the direct measurement of elastic constants in relevant phases and phase mixtures present in HZO thin films provides necessary information for investigations of stress effects on phase stabilization, domain structure, and ferroelectric

This is the author's peer reviewed, accepted manuscript. However, the online version of record will be different from this version once it has been copyedited and typeset PLEASE CITE THIS ARTICLE AS DOI: 10.1063/5.0044702

performance. Additionally, knowledge of the elastic behavior of these ferroelectric materials is critical for emergent piezoMEMS applications, such as resonator device structures.^{26,27}

In this study, the elastic moduli (E) of amorphous and crystalline 20 nm-thick $Hf_{1-x}Zr_xO_2$ $(0 \le x \le 1)$ thin films prepared with TaN electrodes on silicon substrates are directly investigated using picosecond acoustic measurements. The crystallized films comprise pure monoclinic HfO_2 , pure tetragonal ZrO_2 , and phase mixtures in the alloy compositions, which include the ferroelectric orthorhombic phase. The experimental elastic moduli from these measurements are utilized to quantify the stress states of the crystalline 20 nm-thick HZO films through $\sin^2(\psi)$ X-ray diffraction analyses.

Metal-Insulator-Metal (MIM) devices comprising $Hf_{1-x}Zr_xO_2$, with x = 0, 0.31, 0.46, 0.79, and 1, between TaN top and bottom electrodes were prepared. 100 nm-thick TaN bottom electrodes were deposited via DC sputtering from a TaN target onto (001)-oriented silicon substrates under an argon background pressure of 5 mTorr at a power density of 3.3 W cm⁻² with a 45 degree offaxis geometry. 20 nm-thick Hf_{1-x}Zr_xO₂ films were deposited via plasma-enhanced atomic layer (PEALD) 260 °C deposition substrate temperature tetrakis(ethylmethylamido)hafnium (TEMA Hf) and tetrakis(ethylmethylamido)zirconium (TEMA Zr) as hafnium and zirconium precursors, respectively, and an oxygen plasma as the oxidant within an Oxford FlexAL II instrument, as detailed in the supplemental information. The ratio of Hf:Zr cycles within each 10-cycle super cycle was altered to control the film composition. The growth rates were determined to be 1.05 Å/cycle and 1.15 Å/cycle for HfO2 and ZrO2, respectively. Film compositions were determined via X-ray Photoelectron Spectroscopy measurements of fully processed devices, with details provided in the supplemental information. Following HZO deposition, films meant for crystallization received planar, sputtered 20 nm-thick TaN top electrodes and the samples were annealed at 600 °C for 30 seconds under N2 at atmospheric pressure. Following annealing, samples on which electrical analyses were to be performed received 50 nm-thick circular Pd contacts through a shadow mask with diameters spanning 100 – 500 µm via DC sputtering utilizing the same conditions as for the electrodes. Samples were subsequently exposed to an SC-1 etch solution (5:1:1 H₂O:30% H₂O₂ in H₂O:30% NH₄OH in H₂O) at 60 °C for 25 minutes to remove the exposed TaN and define devices for electrical analyses using the Pd contacts as a hard mask. Polarization versus electric field hysteresis This is the author's peer reviewed, accepted manuscript. However, the online version of record will be different from this version once it has been copyedited and typeset PLEASE CITE THIS ARTICLE AS DOI: 10.1063/5.0044702

(P(E), 10 ms test period), current-voltage, and positive up negative down (PUND, 1 ms pulse and 1000 ms delay) measurements were made between 1.0 - 2.5 MV cm⁻¹ using a Radiant Technologies Precision LC II Tester. Capacitance-voltage (CV) measurements were made using a Keysight E4980A LCR meter at 10 kHz with a 50 mV oscillator amplitude. The phase constitution and thickness/density of each of the films were examined using grazing incidence X-ray diffraction (GIXRD) and X-ray reflectivity (XRR), respectively, on samples processed without Pd contacts using a Rigaku SmartLab diffractometer with Cu Kα radiation in a parallel beam configuration. GIXRD was performed with ω fixed at 0.7° and XRR patterns were fit with GSAS-II software.²⁸ 80 nm of aluminum was e-beam evaporated onto each film, which had been measured with GIXRD and XRR to serve as a transducer for picosecond acoustic measurements. The resulting acoustic signatures were fit using LIPRAS line-profile analysis software.²⁹ 2D diffraction patterns were collected on crystallized samples using a Bruker APEXII Duo diffractometer equipped with an Incoatec IµS Cu K α microfocus source and an APEXII CCD area detector with ω fixed at 18 $^{\circ}$. MgO powder was placed on film surfaces for use as a stress-free standard and for sample displacement alignment. Area detector patterns were unwarped using the pyFAI azmithual integration package. 30 $\sin^2(\psi)$ analyses were carried out on the crystallized films using intensity profiles extracted at ψ angles between 0° and 45° relative to the film surface normal to calculate the stress state of each film using the elastic moduli determined from picosecond acoustic measurements.

Figure 1(a) shows the P(E) response measured on each HZO film. Responses were observed to be linear for HfO₂ and ZrO₂, hysteretic for Hf_{0.69}Zr_{0.31}O₂ and Hf_{0.54}Zr_{0.46}O₂, and pinched hysteretic for Hf_{0.21}Zr_{0.79}O₂. The largest polarization was observed for the Hf_{0.54}Zr_{0.46}O₂ film. The pure ZrO₂ film required electric fields in excess of 2.5 MV cm⁻¹ to exhibit the typical field-induced ferroelectric response. Corresponding switching current measurements are available in the supplemental information Figure S1. The remanent polarizations (P_r , from PUND measurements at 2.5 MV cm⁻¹) for each composition within the series are shown in Figure 1(b) and confirm the composition dependence of polarization observed in the P(E) data. These responses are consistent with prior reports on the compositional dependence of polarization response in HZO and suggest non-trivial orthorhombic phase fractions in the Hf_{0.69}Zr_{0.31}O₂ and Hf_{0.54}Zr_{0.46}O₂ films.^{17,18,21}

PLEASE CITE THIS ARTICLE AS DOI: 10.1063/5.0044702

Figure 2 shows GIXRD patterns corresponding to each crystallized film, indicating the phases present at each composition. The diffraction pattern measured on the pure HfO₂ film contained two peaks at 28.6° and 31.9° in 2θ , which were indexed as the ($\bar{1}11$) and (111) monoclinic (m) reflections, respectively. Diffraction patterns measured on the Hf_{0.69}Zr_{0.31}O₂ and $Hf_{0.54}Zr_{0.46}O_2$ films contained an additional peak at 30.7° in 2θ , which was indexed as the superimposed (101) tetragonal/(111) orthorhombic (t/o) reflections, and observed to increase in intensity with increasing ZrO2 concentration. The diffraction patterns measured on the Hf_{0.21}Zr_{0.79}O₂ and pure ZrO₂ films contained only t/o peaks. The t/o peak position increased in diffraction angle in the ZrO2 pattern, which is consistent with previous observations of the diffraction behavior in composition-varied HZO thin films and has been attributed to the tetragonal phase.¹⁹ GIXRD patterns for the un-annealed films lacked distinct Bragg reflections and are available in supplemental information Figure S2. Combined, the GIXRD patterns and electrical measurements suggest that the Hf_{0.54}Zr_{0.46}O₂ film contained the largest orthorhombic phase content: it exhibited the highest measured $P_{\rm I}$ and an intense, low angle t/o diffraction peak. The $Hf_{0.69}Zr_{0.31}O_2$ film, which had the second highest P_r and diffraction peaks corresponding to all three phases, likely had the second largest orthorhombic phase content. The Hf_{0.21}Zr_{0.79}O₂ film had a higher content of the tetragonal phase, as evidenced by the pinched hysteresis response, low P_r , and single t/o diffraction peak. The pure HfO2 and ZrO2 films had diffraction patterns and electrical responses consistent with pure monoclinic and tetragonal phases, respectively. The high field permittivities (2.5 MV cm⁻¹), extracted from CV measurements (supplemental Figure S3), further support a transition from a low permittivity monoclinic phase to higher permittivity orthorhombic and tetragonal phases as the film composition is varied from pure HfO₂ to pure ZrO₂.

XRR measurements of each sample were used to quantify film densities and obtain thickness values. The measurements and associated fits can be found in the supplemental information Figures S4 and S5 for the crystallized and amorphous sample series, respectively. The densities of the crystallized and amorphous films were observed to decrease approximately linearly as the composition changed from pure HfO₂ to pure ZrO₂, as provided in Table I and shown in supplemental information Figure S6 along with the film thicknesses.

The longitudinal speed of sound was extracted from optical pump-probe picosecond acoustic measurements $^{31-33}$ using a two-tint time-domain thermoreflectance system, which is

Publishin

This is the author's peer reviewed, accepted manuscript. However, the online version of record will be different from this version once it has been copyedited and typeset

PLEASE CITE THIS ARTICLE AS DOI: 10.1063/5.0044702

described elsewhere. 34,35 Briefly, the output of a Ti:Sapphire oscillator (100 fs pulses, 80 MHz) is energetically separated into high-energy pump and low-energy probe paths. The pump is electro-optically modulated at 8.4 MHz, and creates a periodic heating event at the surface of the samples coated with aluminum. This heating event also generates a strain pulse that propagates through the film stack, partially transmitting/reflecting at the interfaces between the layers. The reflectivity of the aluminum transducer is interrogated using the probe, which is mechanically delayed ~100 ps following the incident pump pulse. Because the reflectivity of the aluminum is proportional to both temperature and strain, signatures at short pump/probe delay times are indicative of the acoustic propagation times within each layer. Acoustic responses for the 20 nm-thick crystallized HZO films are shown in Figure 3(a), where signatures from the Al/HZO and HZO/TaN interfaces are identified, with equivalent data for the amorphous films provided in supplemental Figure S7. The delay time between these two signatures, τ , represents the round-trip propagation time of the strain wave within the film, as diagrammed in supplemental Figure S8. Gaussian peaks were fit to both acoustic signatures to determine this delay, as shown for the $Hf_{0.54}Zr_{0.46}O_2$ film in supplemental Figure S9. Utilizing the measured film thicknesses, d, and the round-trip propagation times, the longitudinal speed of sound in each film was calculated via $v_L = 2d/\tau$. Elastic moduli were then calculated from the longitudinal wave velocities and the density measurements using Equation (1) with the assumptions of an isotropic randomly oriented, polycrystalline solid or isotropic amorphous layer:³⁶

$$E = \rho v_L^2 \tag{1}$$

Where v_L is the longitudinal speed of sound, ρ is the film density, and E is the elastic modulus of the film. The elastic moduli, provided in Table I and shown in Figure 3(b), were observed to increase with increasing ZrO₂ composition, between 248 ± 6 GPa for the pure monoclinic HfO₂ film and 267 ± 9 GPa for the pure tetragonal ZrO₂ film, with positive deviations from this trend observed for the Hf_{0.69}Zr_{0.31}O₂ (264 ± 8 GPa) and Hf_{0.54}Zr_{0.46}O₂ (274 ± 8 GPa) compositions. The elastic moduli of the amorphous films were observed to increase with increasing ZrO₂ composition, from 211 ± 6 GPa to 302 ± 9 GPa between pure HfO₂ and pure ZrO₂. Additional

PLEASE CITE THIS ARTICLE AS DOI: 10.1063/5.0044702

thickness, density, and sound velocity data for the amorphous films are provided in supplemental Table SI.

Given that the Hf_{0.69}Zr_{0.31}O₂ and Hf_{0.54}Zr_{0.46}O₂ films contained the second largest and largest contents of the orthorhombic phase respectively, according to diffraction and electrical

Given that the $Hf_{0.69}Zr_{0.31}O_2$ and $Hf_{0.54}Zr_{0.46}O_2$ films contained the second largest and largest contents of the orthorhombic phase, respectively, according to diffraction and electrical characterization, these positive deviations from the apparent increase indicate that the orthorhombic phase has an elastic modulus larger than the monoclinic and tetragonal phases. These values are in agreement with DFT predictions, 37,38 and experimental trends between the bulk modulus of the monoclinic and non-ferroelectric orthorhombic phases of HfO_2 . The elastic moduli measured for the $Hf_{0.54}Zr_{0.46}O_2$ film (274 \pm 8 GPa), which possessed the largest content of the orthorhombic phase, is lower than the reported 340 GPa value extracted from fitting of acoustic vibrational responses of 10 nm-thick HZO nano-membrane resonators, 27 and is larger than the reported \sim 170 GPa value measured on 10-100 nm-thick $Hf_{0.55}Zr_{0.45}O_2$ films by atomic force microscopy. These differences may be related to varying phase purities, mechanical boundary conditions, and/or the indirect nature of moduli calculation from these other techniques.

Utilizing measured elastic moduli, $\sin^2(\psi)$ analyses were performed to assess the biaxial stress present in each of the crystalline films following processing. 2D diffraction patterns were collected using an area detector, with an example shown in Figure 4(a) for the Hf_{0.54}Zr_{0.46}O₂ sample. Area detector data were unwarped using the MgO diffraction peaks, with an example shown in supplemental Figure S10. The ($\bar{1}11$) and (111) m (in the case of the HfO₂ film) and (101)/(111) t/o reflections (in the case of the other films) were fit to quantify changes in *d*-spacing with ψ angle relative to film normal, as shown in Figure 4(b) for the Hf_{0.54}Zr_{0.46}O₂ sample. The normalized intensities of the superimposed t/o diffraction peaks, also shown in Figure 4(b) for the Hf_{0.54}Zr_{0.46}O₂ film, were observed to be effectively constant throughout the Debye ring, validating the assumption of a randomly oriented polycrystalline material. A similar lack of texture was observed in all other samples, except pure HfO₂, with the 2D patterns shown in supplemental Figure S11. These observed changes in *d*-spacing with ψ angle were fit using Equations (2) and (3), with the assumption of a randomly oriented, polycrystalline solid with isotropic elastic behavior.⁴¹ Note that this calculation accounts for the biaxial modulus in an equi-biaxially stressed thin film.

This is the author's peer reviewed, accepted manuscript. However, the online version of record will be different from this version once it has been copyedited and typeset PLEASE CITE THIS ARTICLE AS DOI: 10.1063/5.0044702

 $\varepsilon_{\psi} = \frac{I + \nu}{E} \sigma_{\parallel} \sin^2(\psi) - \frac{2\nu}{E} \sigma_{\parallel} \tag{2}$

$$\varepsilon_{\psi} = \frac{d_{\psi} - d_0}{d_0} \tag{3}$$

Where d_{ψ} is the *d*-spacing at each ψ angle, v is Poisson's ratio (assumed to be 0.29^{42-44}), E is the measured elastic modulus for each composition, and $\sigma_{||}$ is the biaxial stress state. The strain-free *d*-spacings (d_0) of the HZO films were calculated to occur at ψ angles (ψ^*) at which Equation (4) was fulfilled:⁴¹

$$\sin(\psi^*) = \sqrt{\frac{2\nu}{1+\nu}} \tag{4}$$

The *d*-spacings of the MgO powder resting on the film surface, shown in supplemental Figures S10 and S12, were not observed to vary with ψ angle, indicating that the observed m/t/o *d*-spacing slopes are not measurement artifacts.

The biaxial stress states of the crystalline films were found to be 2.54 ± 0.6 GPa for the pure HfO₂ film (averaged between the ($\overline{1}11$) and (111) monoclinic peaks), 3.75 ± 0.2 GPa, 4.71 ± 0.4 GPa, and 5.00 ± 0.3 GPa, for the Hf_{0.69}Zr_{0.31}O₂, Hf_{0.54}Zr_{0.46}O₂, and Hf_{0.21}Zr_{0.79}O₂ compositions, respectively, and 5.22 ± 0.5 GPa for the ZrO₂ film. Values utilized for stress quantification can be found in Table I, a discussion of error propagation in all elastic moduli and biaxial stress calculations can be found in the supplemental information, and analogous $\sin^2(\psi)$ analyses can be found for the other samples in supplemental Figure S13. The large tensile biaxial stresses present following processing are consistent with other studies examining stress states of HfO₂-based ferroelectrics grown on binary nitride electrodes and suggest significant stress resulting from thermal expansion mismatch with the silicon substrates.²⁴ Given that monoclinic HfO₂ possesses a smaller coefficient of thermal expansion than tetragonal ZrO₂,⁴⁵ and that clear evidence of monoclinic ferroelastic twin texturing was observed in the 2D diffraction patterns,⁴⁶ it is

PLEASE CITE THIS ARTICLE AS DOI: 10.1063/5.0044702

anticipated that the monoclinic HfO₂ and mixed phase Hf_{0.69}Zr_{0.31}O₂ films could better accommodate thermal strains compared to the other compositions, and thus maintain lower biaxial stress following processing. The texture of the ($\bar{1}11$) and (111) reflections in the pure HfO₂ film does mean that the assumption of a randomly oriented, isotropic crystalline solid used throughout the stress calculations is less valid for this film than for the other compositions. Furthermore, it should be emphasized that all of the crystal structures present in this study are elastically anisotropic. An implicit assumption of the $\sin^2(\psi)$ technique used is that the elastic properties of the planes considered do not significantly differ. The complete elastic compliance tensor for each phase and composition would be necessary to account for any differences and, to date, this information is not available. Regardless, the random orientation of most compositions, linearity of *d*-spacing versus $\sin^2(\psi)$, and use of the same atomic plane in each phase suggests that these results are reliable.

In summary, the elastic moduli of amorphous and crystalline 20 nm-thick $Hf_{1-x}Zr_xO_2$ films have been directly quantified using picosecond acoustic measurements. For the crystallized films, the elastic moduli were found to increase from 248 ± 6 GPa to 267 ± 9 GPa between the monoclinic HfO_2 and tetragonal ZrO_2 films, respectively. The $Hf_{0.69}Zr_{0.31}O_2$ and $Hf_{0.54}Zr_{0.46}O_2$ films, which were determined to have the largest content of orthorhombic phase, exhibited larger elastic moduli of 264 ± 8 GPa and 274 ± 8 GPa, respectively. The larger elastic moduli of films containing the orthorhombic phase is consistent with computational predictions. The moduli of the amorphous films were observed to linearly increase between 211 ± 6 GPa and 302 ± 9 GPa as the composition was varied from pure HfO_2 to pure ZrO_2 . The biaxial stresses of the crystalline films, quantified using their measured elastic moduli values through $\sin^2(\psi)$ analysis, were found to increase from 2.54 ± 0.6 GPa, for pure HfO_2 , to 5.22 ± 0.5 GPa, for pure ZrO_2 . Direct investigation of these elastic properties, through utilization of picosecond acoustic measurements, allows for enhanced analysis of stress effects on phase stability, domain structure, and polarization properties in HfO_2 -based ferroelectric thin films.

The data that support the findings of this study are available within the article and its supplementary material. See supplementary material for a detailed description of the PEALD processing, XPS measurements, error propagation, and supplemental figures.



This is the author's peer reviewed, accepted manuscript. However, the online version of record will be different from this version once it has been copyedited and typeset

PLEASE CITE THIS ARTICLE AS DOI: 10.1063/5.0044702

This work was supported, in part, by the Laboratory Directed Research and Development program at Sandia National Laboratories. Sandia National Laboratories is a multimission laboratory managed and operated by National Technology and Engineering Solutions of Sandia, LLC, a wholly owned subsidiary of Honeywell International, Inc., for the U.S. Department of Energy's National Nuclear Security Administration under contract DE-NA0003525. This paper describes objective technical results and analysis. Any subjective views or opinions that might be expressed in the paper do not necessarily represent the views of the U.S. Department of Energy or the United States Government. This work is also supported, in part, by the Semiconductor Research Corporation's (SRC) Global Research Collaboration Program. This research utilized a PHI VersaProbe III XPS system, which was supported by National Science Foundation Award # 162601. STJ acknowledges support from the National Science Foundation Graduate Research Fellowship Program under award DGE-1842490. DHO is grateful for funding from the National Defense Science and Engineering Graduate (NDSEG) Fellowship. DHO and PEH appreciate funding from the National Science Foundation, Grant Number DMR EPM 2006231. This manuscript has been coauthored by UT-Battelle, LLC, under Contract No. DE-AC05-00OR22725 with the U.S. Department of Energy. The United States Government retains and the publisher, by accepting the article for publication, acknowledges that the United States Government retains a non-exclusive, paid-up, irrevocable, world-wide license to publish or reproduce the published form of this manuscript, or allow others to do so, for United States Government purposes.

PLEASE CITE THIS ARTICLE AS DOI: 10.1063/5.0044702

References: 1 T.S. Bösck

- ¹ T.S. Böscke, J. Müller, D. Bräuhaus, U. Schröder, and U. Böttger, Appl. Phys. Lett. **99**, 102903 (2011).
- ² S. Mueller, S.R. Summerfelt, J. Muller, U. Schroeder, and T. Mikolajick, IEEE Electr. Device L. **33**, 1300 (2012).
- ³ J. Müller, T.S. Böscke, D. Bräuhaus, U. Schröder, U. Böttger, J. Sundqvist, P. Kücher, T. Mikolajick, and L. Frey, Appl. Phys. Lett. 99, 112901 (2011).
- ⁴ L. Chen, T.-Y. Wang, Y.-W. Dai, M.-Y. Cha, H. Zhu, Q.-Q. Sun, S.-J. Ding, P. Zhou, L. Chua, and D.W. Zhang, Nanoscale **10**, 15826 (2018).
- ⁵ Y. Goh and S. Jeon, Nanotechnology **29**, 335201 (2018).
- ⁶ S. Kirbach, K. Kühnel, and W. Weinreich, in 2018 IEEE 18th International Conference on Nanotechnology (IEEE-NANO) (2018), pp. 1–4.
- M. Hoffmann, U. Schroeder, C. Künneth, A. Kersch, S. Starschich, Ulrich Böttger, and T. Mikolajick, Nano Energy 18, 154 (2015).
- ⁸ M. Hoffmann, B. Max, T. Mittmann, U. Schroeder, S. Slesazeck, and T. Mikolajick, in 2018 *IEEE International Electron Devices Meeting (IEDM)* (2018), p. 31.6.1-31.6.4.
- ⁹ M. Hoffmann, F.P.G. Fengler, M. Herzig, T. Mittmann, B. Max, U. Schroeder, R. Negrea, P. Lucian, S. Slesazeck, and T. Mikolajick, Nature 565, 464 (2019).
- ¹⁰ R. Batra, T.D. Huan, G.A. Rossetti, and R. Ramprasad, Chem. Mater. **29**, 9102 (2017).
- ¹¹ R. Batra, T.D. Huan, J.L. Jones, G. Rossetti, and R. Ramprasad, J. Phys. Chem. C **121**, 4139 (2017).
- ¹² C. Künneth, R. Materlik, and A. Kersch, J. Appl. Phys. **121**, 205304 (2017).
- ¹³ S. Starschich and U. Boettger, J. Mater. Chem. C **5**, 333 (2017).

This is the author's peer reviewed, accepted manuscript. However, the online version of record will be different from this version once it has been copyedited and typeset. PLEASE CITE THIS ARTICLE AS DOI: 10.1063/5.0044702

- ¹⁴ M.H. Park, T. Schenk, C.M. Fancher, E.D. Grimley, C. Zhou, C. Richter, J.M. LeBeau, J.L. Jones, T. Mikolajick, and U. Schroeder, J. Mater. Chem. C 5, 4677 (2017).
- ¹⁵ S.J. Kim, D. Narayan, J.-G. Lee, J. Mohan, J.S. Lee, J. Lee, H.S. Kim, Y.-C. Byun, A.T. Lucero, C.D. Young, S.R. Summerfelt, T. San, L. Colombo, and J. Kim, Appl. Phys. Lett. 111, 242901 (2017).
- ¹⁶ T. Shiraishi, K. Katayama, T. Yokouchi, T. Shimizu, T. Oikawa, O. Sakata, H. Uchida, Y. Imai, T. Kiguchi, T.J. Konno, and H. Funakubo, Appl. Phys. Lett. 108, 262904 (2016).
- ¹⁷ J. Müller, T.S. Böscke, U. Schröder, S. Mueller, D. Bräuhaus, U. Böttger, L. Frey, and T. Mikolajick, Nano Lett. 12, 4318 (2012).
- ¹⁸ M.H. Park, H.J. Kim, Y.J. Kim, Y.H. Lee, T. Moon, K.D. Kim, S.D. Hyun, F. Fengler, U. Schroeder, and C.S. Hwang, ACS Appl. Mater. Inter. 8, 15466 (2016).
- ¹⁹ H.A. Hsain, Y. Lee, G. Parsons, and J.L. Jones, Appl. Phys. Lett. **116**, 192901 (2020).
- ²⁰ H. Yu, C.-C. Chung, N. Shewmon, S. Ho, J.H. Carpenter, R. Larrabee, T. Sun, J.L. Jones, H. Ade, B.T. O'Connor, and F. So, Adv. Funct. Mater. 27, 1700461 (2017).
- ²¹ S.W. Smith, A.R. Kitahara, M.A. Rodriguez, M.D. Henry, M.T. Brumbach, and J.F. Ihlefeld, Appl. Phys. Lett. 110, 072901 (2017).
- ²² E.A. Scott, S.W. Smith, M.D. Henry, C.M. Rost, A. Giri, J.T. Gaskins, S.S. Fields, S.T. Jaszewski, J.F. Ihlefeld, and P.E. Hopkins, Appl. Phys. Lett. 113, 192901 (2018).
- ²³ T. Shiraishi, K. Katayama, T. Yokouchi, T. Shimizu, T. Oikawa, O. Sakata, H. Uchida, Y. Imai, T. Kiguchi, T.J. Konno, and H. Funakubo, Mat. Sci. Semicon. Proc. 70, 239 (2017).
- ²⁴ T. Schenk, C.M. Fancher, M.H. Park, C. Richter, C. Künneth, A. Kersch, J.L. Jones, T. Mikolajick, and U. Schroeder, Adv. Electron. Mater. 5, 1900303 (2019).

This is the author's peer reviewed, accepted manuscript. However, the online version of record will be different from this version once it has been copyedited and typeset. PLEASE CITE THIS ARTICLE AS DOI: 10.1063/5.0044702

- ²⁵ E.D. Grimley, T. Schenk, X. Sang, M. Pešić, U. Schroeder, T. Mikolajick, and J.M. LeBeau, Adv. Electron. Mater. 2, 1600173 (2016).
- ²⁶ M. Ghatge, G. Walters, T. Nishida, and R. Tabrizian, Appl. Phys. Lett. **116**, 043501 (2020).
- ²⁷ F. Hakim, M. Ghatge, and R. Tabrizian, Appl. Phys. Lett. **117**, 063502 (2020).
- ²⁸ B.H. Toby and R.B. Von Dreele, J. Appl. Crystallogr. **46**, 544 (2013).
- ²⁹ G. Esteves, K. Ramos, C.M. Fancher, and J.L. Jones, *LIPRAS: Line-Profile Analysis Software* DOI: 10.13140/RG.2.2.29970.25282/3.
- ³⁰ J. Kieffer, V. Valls, N. Blanc, and C. Hennig, J. Synchrotron Radiat. 27, 558 (2020).
- ³¹ J.L. Braun, S.W. King, A. Giri, J.T. Gaskins, M. Sato, T. Fujiseki, H. Fujiwara, and P.E. Hopkins, Appl. Phys. Lett. 109, 191905 (2016).
- ³² C. Thomsen, H.J. Maris, and J. Tauc, Thin Solid Films **154**, 217 (1987).
- ³³ H. -N. Lin, R.J. Stoner, H.J. Maris, and J. Tauc, J. Appl. Phys. **69**, 3816 (1991).
- ³⁴ K. Kang, Y.K. Koh, C. Chiritescu, X. Zheng, and D.G. Cahill, Rev. Sci. Instrum. **79**, 114901 (2008).
- ³⁵ D.H. Olson, J.T. Gaskins, J.A. Tomko, E.J. Opila, R.A. Golden, G.J.K. Harrington, A.L. Chamberlain, and P.E. Hopkins, Scripta Mater. 177, 214 (2020).
- ³⁶ R. Newnham, *Properties of Materials: Anisotropy, Symmetry, Structure* (Oxford University Press, 2005).
- ³⁷ R. Materlik, C. Künneth, and A. Kersch, J. Appl. Phys. **117**, 134109 (2015).
- ³⁸ M.H. Park, Y.H. Lee, H.J. Kim, T. Schenk, W. Lee, K.D. Kim, F.P.G. Fengler, T. Mikolajick, U. Schroeder, and C.S. Hwang, Nanoscale 14 (2017).
- ³⁹ Y. Al-Khatatbeh, K.K.M. Lee, and B. Kiefer, Phys. Rev. B **82**, 144106 (2010).
- ⁴⁰ L. Bolotov, N. Uchida, and S. Migita, AIP Adv. **11**, 015216 (2021).

This is the author's peer reviewed, accepted manuscript. However, the online version of record will be different from this version once it has been copyedited and typeset. PLEASE CITE THIS ARTICLE AS DOI: 10.1063/5.0044702

 $^{^{41}}$ M. Birkholz, Thin Film Analysis by X-Ray Scattering (Wiley - VCH, KGaA, Weinheim, 2006).

⁴² S.L. Dole, O. Hunter, and C.J. Wooge, J. Am. Ceram. Soc. **60**, 488 (1977).

⁴³ X.-S. Zhao, S.-L. Shang, Z.-K. Liu, and J.-Y. Shen, J. Nucl. Mater. **415**, 13 (2011).

⁴⁴ A. SelCuk and A. Atkinson, J. Eur. Ceram. Soc. **17**, 1523 (1997).

⁴⁵ R.P. Haggerty, P. Sarin, Z.D. Apostolov, P.E. Driemeyer, and W.M. Kriven, J. Am. Ceram. Soc. **97**, 2213 (2014).

⁴⁶ B.M. Hudak, S.W. Depner, G.R. Waetzig, A. Talapatra, R. Arroyave, S. Banerjee, and B.S. Guiton, Nat. Commun. **8**, 15316 (2017).

This is the author's peer reviewed, accepted manuscript. However, the online version of record will be different from this version once it has been copyedited and typeset PLEASE CITE THIS ARTICLE AS DOI: 10.1063/5.0044702

Captions:

- **FIG. 1.** (a) P(E) measurements of HfO₂ (grey), Hf_{0.69}Zr_{0.31}O₂ (blue), Hf_{0.54}Zr_{0.46}O₂ (orange), Hf_{0.21}Zr_{0.79}O₂ (purple), and ZrO₂ (green) films. (b) P_r extracted from PUND measurements.
- $\label{eq:FIG. 2. GIXRD patterns measured on HfO2 (grey), Hf0.69Zr0.31O2 (blue), Hf0.54Zr0.46O2 (orange), Hf0.21Zr0.79O2 (purple), and ZrO2 (green) films.}$
- **FIG. 3.** (a) Acoustic responses measured on crystallized HfO₂ (grey), Hf $_{0.69}$ Zr $_{0.31}$ O₂ (blue), Hf $_{0.54}$ Zr $_{0.46}$ O₂ (orange), Hf $_{0.21}$ Zr $_{0.79}$ O₂ (purple), and ZrO₂ (green) films, with signatures corresponding to the Al/HZO and HZO/TaN interfaces indicated. (b) Elastic moduli calculated for crystallized (orange circles) and amorphous (blue squares) HZO films.
- **FIG. 4.** (a) 2D XRD pattern measured on the Hf_{0.69}Zr_{0.31}O₂ sample with indexed m, t/o and MgO Debye rings indicated. (b) Change in t/o *d*-spacing with ψ angle relative to film normal (filled blue circles, left axis) with associated linear fit (red dotted line) used to calculate biaxial stress magnitude and normalized peak intensities (open blue circles, right axis) for the Hf_{0.69}Zr_{0.31}O₂ film.



PLEASE CITE THIS ARTICLE AS DOI: 10.1063/5.0044702

This is the author's peer reviewed, accepted manuscript. However, the online version of record will be different from this version once it has been copyedited and typeset.

Tables:

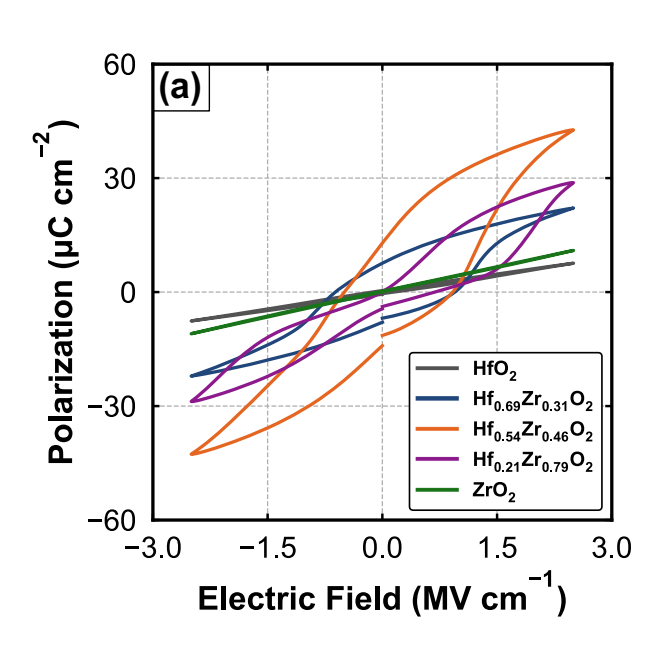
TABLE I. Calculated elastic moduli and biaxial stress magnitudes along with parameters used for calculations, remanent polarizations, and relative permittivities for each HZO composition. * HfO₂ area detector data indicated preferred orientation. * Value represents the average of calculations from both ($\bar{1}11$) and (111) monoclinic peaks.

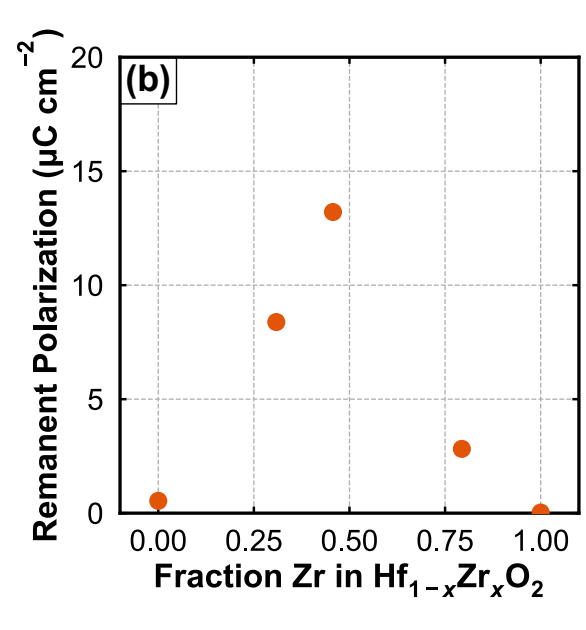
	HfO_2	$Hf_{0.69}Zr_{0.31}O_2$	$Hf_{0.54}Zr_{0.46}O_2$	$Hf_{0.21}Zr_{0.79}O_2$	ZrO_2
Thickness (nm)	20.04 ± 0.30	19.58 ± 0.29	19.37 ± 0.29	20.73 ± 0.31	21.60 ± 0.32
$v_L (\mathrm{m \ s^{-1}})$	5392 ± 96	5788 ± 115	5984 ± 114	6164 ± 110	6656 ± 151
τ (ps)	7.43 ± 0.07	6.76 ± 0.09	6.47 ± 0.08	6.72 ± 0.07	6.37 ± 0.11
ho (g cm ⁻³)	8.55 ± 0.03	7.90 ± 0.04	7.67 ± 0.04	6.82 ± 0.06	6.04 ± 0.05
$P_{\rm r}$ ($\mu {\rm C~cm^{-2}}$, at 2.5 MV cm ⁻¹)	0.54	8.38	14.01	2.82	0.03
ϵ_r (at 2.5 MV cm $^{\text{-1}},10\text{ kHz})$	23.6	34.1	51.1	60.3	42.7
E (GPa, Amorphous)	211 ± 6	226 ± 7	267 ± 10	264 ± 8	302 ± 9
E (GPa, Crystallized)	$*248 \pm 6$	264 ± 8	274 ± 8	259 ± 7	267 ± 9
σ (GPa)	$*,^{\dagger}2.54 \pm 0.6$	3.75 ± 0.2	4.71 ± 0.4	5.00 ± 0.3	5.22 ± 0.5



This is the author's peer reviewed, accepted manuscript. However, the online version of record will be different from this version once it has been copyedited and typeset.





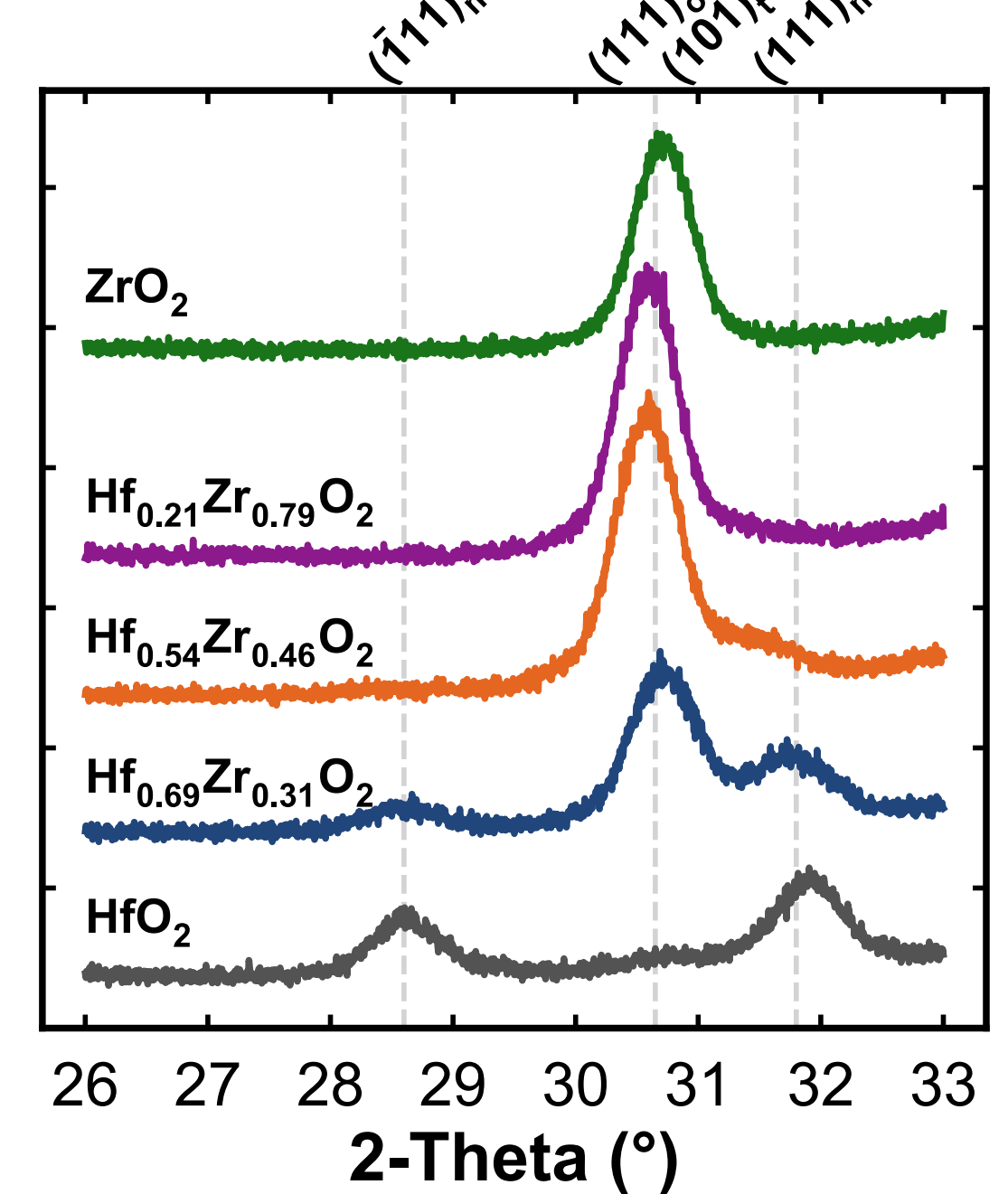




This is the author's peer reviewed, accepted manuscript. However, the online version of record will be different from this version once it has been copyedited and typeset.

PLEASE CITE THIS ARTICLE AS DOI: 10.1063/5.0044702

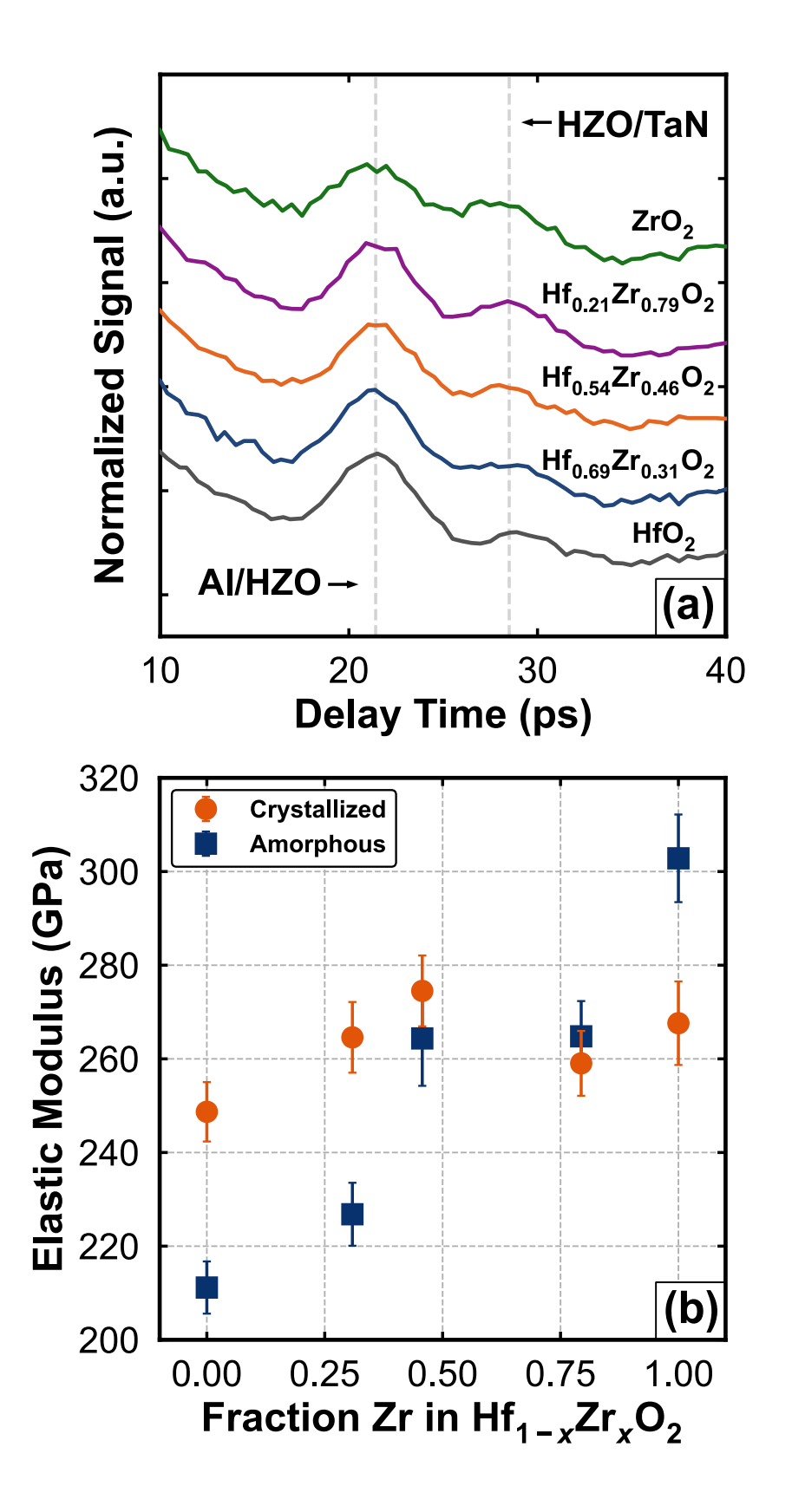






This is the author's peer reviewed, accepted manuscript. However, the online version of record will be different from this version once it has been copyedited and typeset.

PLEASE CITE THIS ARTICLE AS DOI: 10.1063/5.0044702





This is the author's peer reviewed, accepted manuscript. However, the online version of record will be different from this version once it has been copyedited and typeset.



